Structural Characterization of the L-to-M Transition of the Bacteriorhodopsin Photocycle

Felicia M. Hendrickson, Frederick Burkard, and Robert M. Glaeser
Life Sciences Division, Donner Laboratory, Lawrence Berkeley National Laboratory, and Department of Molecular and Cell Biology, Stanley/Donner ASU, University of California, Berkeley, California 94720 USA

ABSTRACT Structural intermediates occurring in the photocycle of wild-type bacteriorhodopsin are trapped by illuminating hydrated, glucose-embedded purple membrane at 170K, 220K, 230K, and 240K. We characterize light-induced changes in protein conformation by electron diffraction difference Fourier maps, and relate these to previous work on photocycle intermediates by infrared (FTIR) spectroscopy. Samples illuminated at 170K are confirmed by FTIR spectroscopy to be in the L state; a difference Fourier projection map shows no structural change within the 0.35-nm resolution limit of our data. Difference maps obtained with samples illuminated at 220K, 230K, and 240K, respectively, reveal a progressively larger structural response in helix F when the protein is still in the M state, as judged by the FTIR spectra. Consistent with previous structural studies, an adjustment in the position or in the degree of ordering of helix G accompanies this motion. The model of the photocycle emerging from this and previous studies is that bacteriorhodopsin experiences minimal change in protein structure until a proton is transferred from the Schiff base to Asp^{85}. The M intermediate then undergoes a conformational evolution that opens a hydrated "half-channel," allowing the subsequent reprotonation of the Schiff base by Asp^{96}.

INTRODUCTION

Bacteriorhodopsin (bR), the 26-kDa light-driven proton pump of *Halobacterium salinarium*, is a transmembrane protein arranged with native lipids in two-dimensional crystalline patches called purple membrane. The structure of bR in the light-adapted resting state (bR_{568}) was determined by Henderson et al. (1990) from electron crystallographic data, and the atomic model has been refined to a nearly isotropic resolution of 0.35 nm (Grigorieff et al., 1996). High-resolution features of this model have been confirmed and extended by an independent electron crystallographic study (Kimura et al., 1997) and by an x-ray diffraction study (Pebay-Peyrouba et al., 1997). A retinal molecule, which lies buried in the middle of seven transmembrane helices (A–G), forms a protonated Schiff base with Lys^{216} on helix G. The atomic model of bR_{568} reveals that the interior of the protein is overwhelmingly hydrophobic on the cytoplasmic side of the Schiff base, whereas several polar residues form an apparently hydrated "half-channel" that reaches to the Schiff base from the extracellular side of the membrane. This implies that in the resting state, the buried Schiff base has access to the extracellular side of the membrane but not to the cytoplasmic side.

Upon absorption of light, the all-*trans* retinal group isomerizes about the C_{13}-C_{14} double bond, adjacent to the Schiff base formed between the retinal C_{15} and the ϵ-NH_2 of Lys^{216}. The protein then spontaneously progresses back to the resting state through a photocycle in which one proton is released into the extracellular medium, and another is taken up from the cytoplasm. Intermediate states in this photocycle have distinct absorption spectra in the visible, occurring in the following sequence (maxima are denoted by subscripts): $bR_{568} \rightarrow K_{610} \rightarrow L_{550} \rightarrow M_{412} \rightarrow N_{550} \rightarrow O_{640} \rightarrow bR_{568}$ (Lozier et al., 1975; also see Mathies, 1991; Lanyi, 1993; Ebrey, 1993; Rothschild and Sonar, 1995; for reviews). In the L $\rightarrow$ M transition, the Schiff base loses its proton to nearby Asp^{85}, located toward the extracellular surface (Henderson et al., 1990), triggering the release of a proton into the medium, possibly from Glu^{204} (Brown et al., 1995). In the M $\rightarrow$ N transition the Schiff base is reprotonated in a step that involves proton uptake from the cytoplasmic side of the membrane.

To further understand how bR functions as an ion pump, we must determine how the deprotonation and reprotonation of the Schiff base can occur, respectively, first from one side of the membrane and then from the other in the L $\rightarrow$ M $\rightarrow$ N sequence. Because the isomerization state of the retinal cofactor remains 13-*cis*, 14-s-*trans*, 15-*anti* throughout this sequence (Braiman and Mathies, 1980; Fodor et al., 1988a,b; Ames et al., 1989; Farrar et al., 1993), and does not return to the all-*trans* configuration until the N $\rightarrow$ O transition (Smith et al., 1983), thermally activated changes in protein conformation, rather than repositioning of the Schiff base, are likely to provide the mechanism for this switch.

A variety of diffraction methods have been used to detect conformational changes occurring at different stages of the photocycle. Neutron (Dencher et al., 1989) and x-ray (Koch et al., 1991; Nakasako et al., 1991) experiments have shown that the most intense and reproducible difference peak in the M-minus-bR_{568} difference maps is a positive peak that occurs at the position of helix G. Using high-resolution electron crystallography, Subramaniam et al. (1993) confirmed this observation. They also found that the M-minus-bR_{568} difference map of the D96G mutant has an equally

Received for publication 29 January 1998 and in final form 15 May 1998.
Address reprint requests to Dr. Felicia Hendrickson, Life Sciences Division, University of California, Donner Laboratory, LBNL, Berkeley, CA 94720. Tel.: 510-486-6597; Fax: 510-486-6488; E-mail: fmh@xtalu.lbl.gov.

0006-3495/98/09/1446/09 $2.00

prominent positive/negative pair of peaks located at the position of helix F. The analysis of data from slightly tilted D96G specimens indicated that all of these structural changes occur in the cytoplasmic half of the molecule. The authors interpreted these changes as an increase in ordered structure in helix G and an outward tilting of the cytoplasmic half of helix F.

The structural changes detected by Subramaniam et al. (1993) may be characteristic of two distinct and sequential steps in the photocycle. The apparent ordering of helix G is detected in the M intermediate of wild-type bR (Subramaniam et al, 1993). The next step would correspond to the positive/negative peak pair observed in the N intermediate of the mutants F219L (Vonck, 1996) and F171C (Kamikubo et al., 1996) and in the M state of the D96G mutant (Subramaniam et al., 1993). In the latter case the protein is believed to be stalled in an N-like conformation, whereas the Schiff base remains deprotonated because of the absence of an acid group at position 96; this state has been called the M_N state (Sasaki et al., 1992).

Events in the photocycle leading up to M are not well understood. Furthermore, the use of different conditions for trapping the M and M_N substates by many investigators has left the question of their structural differences somewhat unclear. To investigate the question of what structural changes occur in the L state, we recorded Fourier transform infrared (FTIR) spectra and collected electron diffraction data to 0.35-nm resolution from glucose-embedded specimens at 170K. To further characterize the L $\rightarrow$ M transition, we also collected FTIR and electron diffraction data from specimens illuminated at 220K, 230K, and 240K, respectively. We observe no movement of helix G in the L state, and find that helix F begins to tilt before the formation of substantial amounts of M_N.

MATERIALS AND METHODS

Purple membrane was isolated from *Halobacterium salinarium* strain ET1001 by the protocol of Oesterhelt and Stoeckenius (1974).

For FTIR spectroscopy, hydrated, glucose-embedded films of purple membrane with an optical density of 0.4 to 0.8 at 1660 cm^{-1} were prepared on CaF_2 windows and equilibrated at a relative humidity of 81% as described by Perkins et al. (1992). Spectra were taken at 2 cm^{-1} resolution on a Mattson Galaxy 3000 FTIR spectrometer (Mattson Instruments, Madison, WI). Sealed specimens were mounted in a home-made cryostat, which was cooled by an adjustable flow of cold nitrogen. Temperatures were controlled to within 1°C. The cryostat is fitted with a light pipe from a mercury lamp, and with an adapter for holding filters. Specimens were rotated in a precision mount while cold, either to be oriented perpendicular to the infrared beam for spectroscopy, or to be orientated perpendicular to the actinic light beam for illumination.

To obtain L-minus-bR FTIR difference spectra, we collected sets of 250 scans at 170K, one set before illumination, and the other immediately after illumination with red light (610 nm cut-on glass filter; Oriel Corp., Stratford, CT) for 2 min. Difference spectra for the M intermediate and for the bR-like photoproduct generated by illuminating the M intermediate with blue light were recorded similarly: sets of 150 scans were taken before illumination at the desired temperature, after illumination for 3 s with green light (peak transmittance 520 nm filter), and after illumination for 3 s with green light followed by 3 s with blue light (peak transmittance 400 nm filter). The intensity of the green light was reduced by the use of neutral density filters to the lowest level, which still produced the maximum response in the 1527 cm^{-1} band in the FTIR difference spectrum. This precaution was taken to minimize any increase in sample temperature due to the illumination.

Purple membranes were fused to form large crystals (diameter ≥ 3 μm) suitable for electron diffraction (Baldwin and Henderson, 1984). We have found that delaying the addition of dodecyltrimethylammonium chloride by ~36 h seems to reduce the tendency of the crystals to stick to one another.

We prepared glucose-embedded purple membrane specimens for electron diffraction essentially as described by Han et al. (1994): for each specimen a square of carbon film was floated from mica onto the surface of a 3–4.5% solution of glucose in 10 mM 3-[*N*-morpholino]propanesulfonic acid buffer, pH 6.7, containing 6 mM octyl glucoside. A 300-mesh molybdenum grid was dipped into the glucose solution and used to pick up the floating carbon film. The volume of the drop captured by the grid in this way was adjusted by eye to ~2 μl, and 1.5 μl of fused purple membrane (3 mg/ml in fusion buffer) was injected into the glucose droplet from the back side of the grid. After mixing, the grid was blotted on filter paper and placed for $\geq$15 min in a stream of air humidified to 81% relative humidity (r.h.), using the home-built plunge-freezing device described in Fig. 1. After equilibration of the sample at high humidity, the grid was illuminated in place with white light for 10 s to ensure a high percentage of light-adapted bR molecules, and then plunged into liquid nitrogen after 5 s in the dark. The plunging step and subsequent manipulations were performed in dim red light, except as stipulated below, to minimize contamination of the resting state by unwanted photocycle intermediates.

The trapping of photocycle intermediates on electron microscope grids has been described previously (Han et al., 1994), and details of that procedure have been further optimized in the course of this work. The specimen grid is transferred into a Gatan cryo-specimen holder under liquid nitrogen, and then warmed to 163K and exposed in the dark to room air for 90 s. The purpose of this step is to condense a protective coating of frost onto the grid to prevent subsequent dessication of the sample by cold nitrogen gas. The specimen holder is then inserted into a home-made illumination chamber, where it is equilibrated to the desired temperature with cold nitrogen gas. When the temperatures of the flowing nitrogen gas and of the Gatan probe have both stabilized to the target value, the grid is illuminated under the same conditions as described for the FTIR experiments described above. At each temperature, specimens of bR_{568} are prepared in an identical manner, except that the grids are not illuminated when held at the target temperature. Grids are rapidly cooled to liquid nitrogen temperature after illumination, and their temperature is maintained

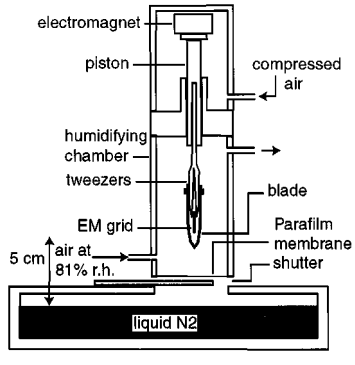

FIGURE 1 Device for plunge-freezing specimens for electron microscopy. The grid equilibrates to 81% r. h. in the humidifying chamber. Activation of a circuit breaker simultaneously releases the piston from the electromagnet and opens the shutter over the entrance to the liquid nitrogen bath. The blade cuts through the parafilm membrane, allowing the grid to be transferred from the humidifying chamber to the bath of liquid nitrogen with minimal exposure to ambient humidity.

below 110 K during cryotransfer into the vacuum of the electron microscope. The specimen temperature is briefly raised to 173K when in vacuum, however, to sublime the ice that was intentionally condensed onto it.

Electron diffraction was performed on a JEOL 4000 EX electron microscope, using an accelerating voltage of 400 keV. Specimens were nominally untilted during data collection. The beam size was adjusted to a diameter of 3 μm when diffraction patterns were recorded. The accumulated electron exposure was 10 electron/Å^2, which is about half the dose necessary to completely fade the (4, 3) Bragg reflection at low temperature and 400 keV. Diffraction patterns were recorded on a Gatan 2048 $\times$ 2048 multiscan charge-coupled device (CCD) camera; only those patterns showing good diffraction intensity to at least the 21st order (0.26 nm) were saved to disk.

We used a suite of programs initially developed by Baldwin and Henderson (1984) to index each pattern, to measure the background-subtracted spot intensities, and to fit these intensities to a set of reference curves (Ceska and Henderson, 1990). Merging our diffraction intensities to the reference data provided estimates of temperature factors and twin proportions. These two parameters, along with R_{merge} and Friedel R factors, were used to decide which patterns would be accepted for further analysis. Initially patterns were accepted according to the following criteria: relative temperature factor ≤ 2; highest twin component $\geq 90\%$; Friedel R factor $\leq 16\%$; and $R_{merge} \leq 30\%$. Once all of the patterns collected from the same kind of sample had been merged, those patterns with R_{merge} values more than two standard deviations away from the mean R_{merge} were rejected as outliers. The removal of R_{merge} outliers resulted in the rejection of no more than 10% of the patterns that had met the first set of criteria. New lattice-line curves were then fitted to the diffraction intensities, and structure factor amplitudes were derived from the numerical values of the newly fitted curves.

The data used to calculate difference maps were confined to those Bragg reflections that lie within the resolution range of 1.5–0.35 nm. Differences in amplitudes for the (h,k,0) structure factors were calculated, and difference amplitudes were combined with the original phase data for bR (Henderson et al., 1990) to produce difference Fourier projection maps, with contour levels set at one-tenth the value used in the projection map of bR shown in Fig. 2 *A*. The noise level in the difference Fourier maps was estimated by splitting each data set into two independent halves, and using the data to calculate separate sets of lattice-line curves. From these we calculated self-difference projection maps, which were contoured at the same level as was used for the real difference maps.

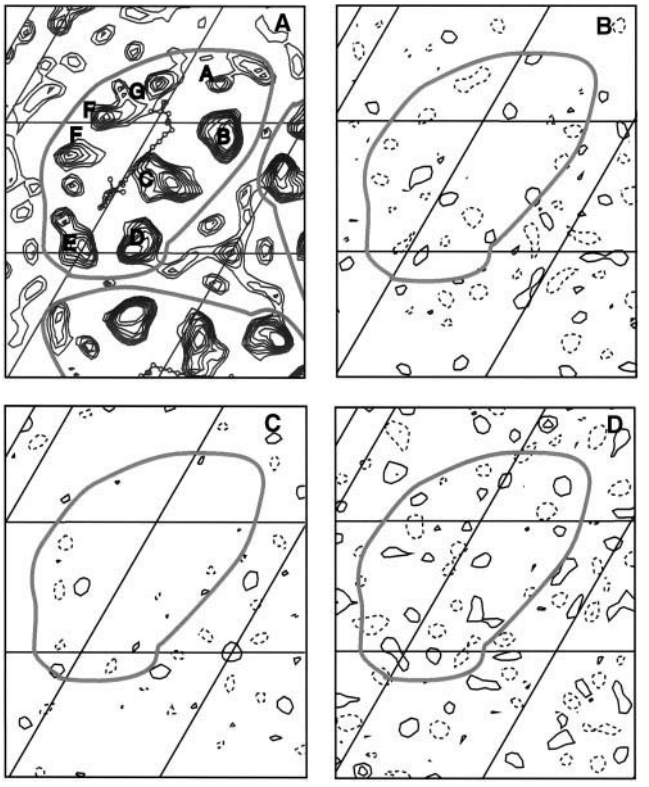

FIGURE 2 The L intermediate of bacteriorhodopsin trapped at 170K. (*A*) Projection map of bR_{568} at 170K. Only the positive contours of the map are shown. The stick-and-ball figure represents the position of the retinal chromophore in the atomic model of Grigorieff et al. (1996). The outlines in gray depict an approximation of the protein envelope of three bR molecules in the plane of the membrane; the seven helices are labeled in one monomer. Grid lines are separated by 20.8 Å, or one-third of a unit cell. (*B*) Difference Fourier L-minus-bR_{568} projection map. A set of $F(h,k,0)$ amplitudes was derived from 32 diffraction patterns collected from unilluminated purple membrane at 170K, and a second set was derived from 46 L diffraction patterns collected from illuminated specimens. (*C*) Self-difference map using independent halves of the bR_{568}, 170K data set. The map provides an estimate of the noise present in the data. (*D*) Self-difference map using independent halves of the L data set.

RESULTS

The difference Fourier projection map for the L intermediate shows no significant structural change relative to the light-adapted, resting state reference shown in Fig. 2 *A*. Difference peaks in the L-minus-bR_{568} difference map (Fig. 2 *B*) are comparable to those found in the self-difference maps bR-minus-bR (Fig. 2 *C*) and L-minus-L (Fig. 2 *D*) in terms of both abundance and contour height. Hence there is no signal in the L-minus-bR map above the conservative estimate of the noise level given by the self-difference maps.

The FTIR difference spectrum of glucose-embedded specimens shown in Fig. 3 confirms that the conditions described above do in fact trap bR in the L state. Several distinguishing features replicate those of L-bR spectra published by other groups working between 170K and 298K (Braiman et al., 1988, 1991; Gerwert et al., 1989; Hessling et al., 1993; Ormos et al., 1992), including a composite negative peak at 1740 cm^{-1} (assigned to Asp^{96} and Asp^{115}), a negative peak at 1640 cm^{-1} (assigned to the Schiff base C=N), and a positive peak at 1395 cm^{-1} associated with a protonated Schiff base. Small changes in the amide I region are also seen in our spectrum at 1660 cm^{-1} and 1670 cm^{-1}, in agreement with Braiman et al. (1991) and Hessling et al. (1993), but at odds with Gerwert et al. (1989) and Ormos et al. (1992), who detected only a 1660 cm^{-1} peak in the amide I region. The peaks in the amide I and II regions are smaller than those seen in later intermediates of the photocycle.

The strong negative peak at 1527 cm^{-1} signals the formation of the 13-*cis* isomer of retinal. In control experiments in which L and M are formed from the same film, the depth of this peak in the L-minus-bR spectra is ~70% of that observed in the M-minus-bR spectra (data not shown). Because our conditions were shown previously to result in more than 90% occupancy for the M intermediate (Perkins et al., 1992), we estimate an occupancy of not less than 65% for the L intermediate.

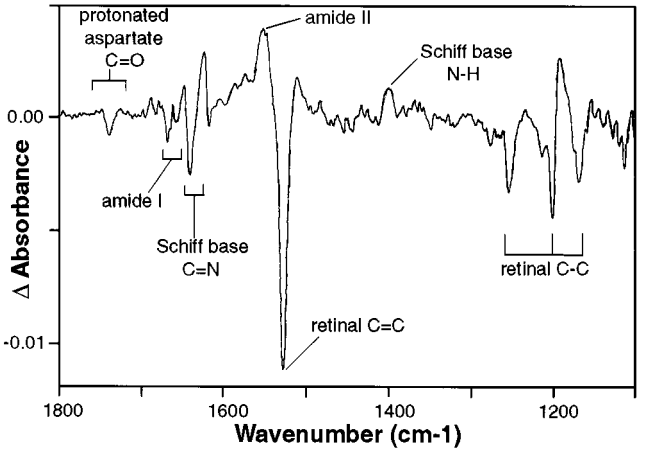

FIGURE 3 Illuminated-minus-unilluminated FTIR difference spectrum at 170K between 1800 and 1100 cm^{-1}. The spectrum shown is an average of 500 individual scans. The positions of the absorbance maxima of the vibrational modes of some important chemical groups (Braiman et al., 1988; Rothschild, 1992) are noted.

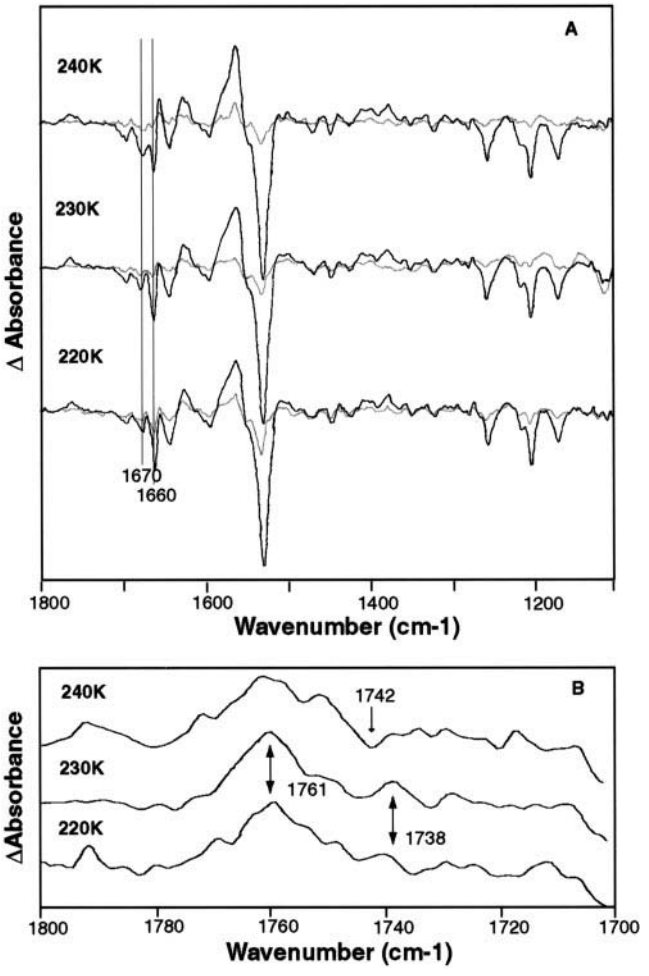

FIGURE 4 Illuminated-minus-unilluminated FTIR difference spectra at 240K, 230K, and 220K. (*A*) Spectra recorded between 1800 and 1100 cm^{-1}. The spectra collected at 240K and 220K were normalized to the 230K spectrum (scaled by 1.04 and 1.40, respectively) so that the intensity of the negative peak at 1527 cm^{-1} is −0.0227 for all three. The spectra in black were obtained by illumination with green light only, whereas those in gray show the extent of photoreversal resulting from green, then blue illumination. (*B*) The same spectra as shown in black in *A*, but confined to between 1800 and 1700 cm^{-1} to magnify the protonated aspartate C═O stretch region. At 240K and 230K a total of 750 individual scans were collected for each illumination condition; at 220K, 600 scans were taken.

Illumination of glucose-embedded samples at 240K produces a mixture of M and M_N intermediates, which we infer from the presence of bands at both 1660 cm^{-1} and 1670 cm^{-1} at the top of Fig. 4 *A*. As noted by Sasaki et al. (1992), the two M species can be distinguished by their amide I signatures: the M intermediate has a negative peak at 1660 cm^{-1}, whereas the M_N-state intermediate has N-like features: a negative peak at 1670 cm^{-1}, as well as a much higher positive peak at 1650 cm^{-1}. This key spectroscopic signature has also been used by Kamikubo et al. (1997) to identify a mixture of M- and N-like protein structures in the M state formed by the D96N mutant at high pH and 81% relative humidity. Both the 1670 cm^{-1} and 1650 cm^{-1} peaks are very weak for our samples illuminated at 230K and 220K (Fig. 4 *A*), whereas they are prominent components for samples illuminated at 240K.

Similarly, at 230K we obtain peaks diagnostic for the M state in the aspartate carboxylic acid C═O stretch region (Fig. 4 *B*), at 1761 cm^{-1} and 1738 cm^{-1} (Braiman et al., 1988; Rothschild, 1992). At 240K, however, some red-shifting of the 1761 cm^{-1} peak as well as the appearance of a negative peak at 1742 cm^{-1}, both associated with the N state (Ormos et al., 1992; Hessling et al., 1993), are evident. The spectrum obtained at 220K is again similar to the 230K spectrum in this region.

Photointermediates with a deprotonated Schiff base (that is, all "M" substates) absorb strongly at 410 nm, and can be photoreversed to the ground state by blue light (Litvin and Balashov, 1977). The FTIR difference spectra we obtain between 240K and 230K are almost completely reversed to the baseline by illuminating samples with blue light (Fig. 4 *A*, *gray lines*), demonstrating that little if any L_{550} or N_{550} is trapped in glucose-embedded specimens at these temperatures. This confirms and extends the conclusion of Vonck et al. (1994). The retinal and amide I bands are noticeably more resistant to photoreversal at 220K than at the higher temperatures.

Because the ratio of the 1670 cm^{-1} and 1660 cm^{-1} peak values at 240K is somewhat less than 1:1, the proportion of M_N present would seem to be not higher than ~40%. To get a more accurate estimate of the fractions of M and M_N trapped at 240K, we tested various linear combinations of published M-minus-bR and N-minus-bR spectra (Ormos et al., 1992) for their correlation to our M-minus-bR spectra at 240K, 230K, and 220K (Fig. 5). In the range 1600 cm^{-1} to 1700 cm^{-1}, where absorption by amide groups and the Schiff base C═N is dominant (see Fig. 3), samples illuminated at 220K and 230K are most similar to high proportions of M, 100% and 95%, respectively (Fig. 5). Those

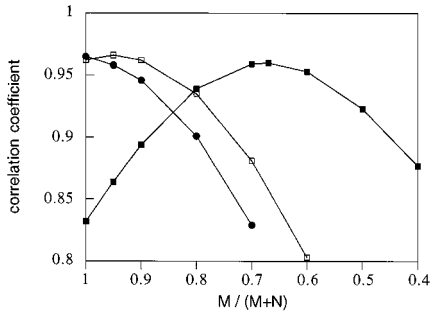

FIGURE 5 Correlation coefficients ($[\Sigma xy - ((\Sigma x_i \Sigma y_i)/N)]/[(\Sigma x_i^2 - (\Sigma x_i \Sigma x_i)/N)(\Sigma y_i^2 - (\Sigma y_i \Sigma y_i)/N)]^{1/2}$) for the illuminated-minus-unilluminated FTIR difference spectra collected at either 240K (■), 230K (□), or 220K (●), and linear combinations of the M-minus-bR_{568} and N-minus-bR_{568} spectra published by Ormos et al. (1992) in two regions: (*A*) between 1700 and 1600 cm^{-1}; (*B*) between 1800 and 1700 cm^{-1}. The ordinate axis shows the decreasing proportion of the M-minus-bR568 spectrum in the linear combinations tested.

illuminated at 240K are quite different, showing the highest correlation, with a 2:1 ratio of M:M_N.

The electron diffraction difference map for samples illuminated at 240K (Fig. 6 *A*) shows a prominent positive peak and a smaller negative peak on helix G (G1,G2), along with a positive/negative pair of peaks on helix F (F1,F2), the latter being identified with tilting of the cytoplasmic portion of helix F. The low noise levels shown for the self-difference maps in Fig. 6, *B* and *C*, demonstrate that the peaks on helix F and helix G in Fig. 6 *A* give a meaningful representation of the light-induced structural changes produced under our conditions. Nevertheless, the respective occupancies of peaks G1, F1, and F2 are apparently no more than half that obtained from the F219L mutant trapped in the N state (Vonck, 1996) or from the D96G mutant trapped in the M_N state (Subramaniam et al., 1993). Samples for both of the latter studies were illuminated at higher temperatures than used here. The lower occupancy of the helix F peaks found here is fully consistent with our FTIR spectra, described above, which show that at 240K we obtain a partial occupancy, ~33%, of the M_N state. The occupancy of the peak on helix G is also relatively low. We now know that this is due to spontaneous partial ordering of the cytoplasmic half of G, which occurs at low temperature even before illumination, leaving a smaller amount of light-induced change that can occur (Hendrickson and Glaeser, manuscript in preparation; also see below).

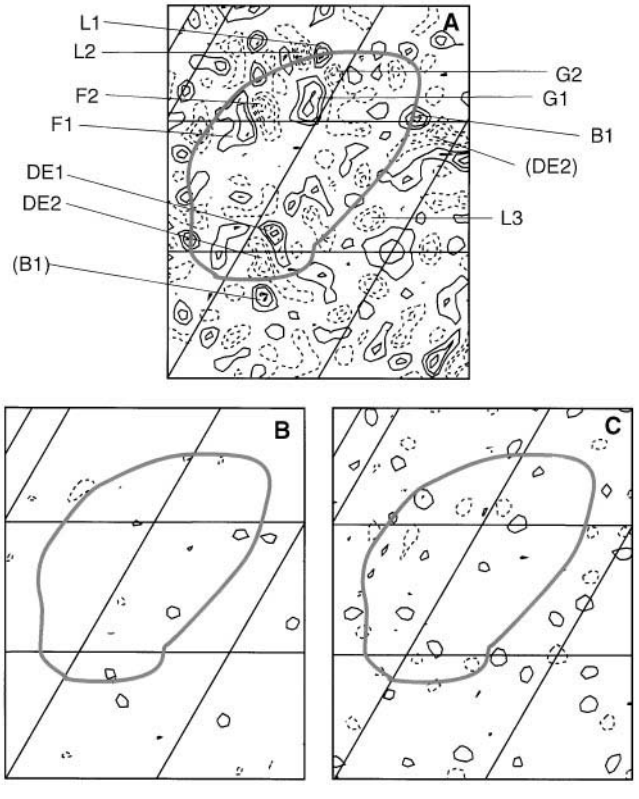

FIGURE 6 Projection map showing light-induced structural changes in bR at 240K. (*A*) Difference Fourier map obtained from 28 diffraction patterns collected from illuminated samples and 45 patterns collected from unilluminated samples. Peaks of at least three contour levels are labeled to facilitate discussion in the text. (*B* and *C*) Self-difference maps using independent halves of the unilluminated and illuminated data sets, respectively.

In addition to the difference peaks associated with helices F and G, significant peaks are also found near projected positions of helices that contact one another at the monomer-monomer interface. These peaks, labeled B1, DE1, and DE2 in Fig. 6 *A*, suggest a light-induced adjustment of helices from adjacent monomers that pack against each other within each trimer. Several peaks of significant contour height are also found outside the protein envelope, and presumably represent the rearrangement of well-ordered lipids. Three of these are labeled L1–3 in Fig. 6 *A*.

Illumination of samples at 230K produces structural changes within the protein envelope very much like those seen at 240K (Fig. 7 *A*; compare Fig. 6 *A*). However, there is an amplification of a positive/negative pair of peaks just below B1, and peak F2 is more compact. A more subtle difference occurs in the shapes of peaks F1 and G1. In contrast, peaks B1 and G2 are virtually identical to their counterparts at 240K. The small amount of noise in these samples (Fig. 7 *B*) indicates that difference peaks with two or more contour levels are highly significant.

Samples illuminated at 220K undergo similar structural changes, at least within the protein envelope (Fig. 7 *C*). In Fig. 7 *C* peaks G1 and F1 are differently shaped than in Fig. 7 *A*, and F2 has moved somewhat, whereas peaks G2, L1, L2, B1, DE1, and DE2 are essentially unaltered. As before, the level of noise in the data is quite low (Fig. 7 *D*).

To convey most clearly the information present in our diffraction data between 240K and 220K, we chose to use the bR_{568} data set collected at 240K for all three M-minus-bR difference maps (Figs. 6 *A* and 7, *A* and *C*). As noted above, spontaneous structural changes occur in unilluminated purple membrane samples equilibrated at low temperatures. This is particularly true near the glass transition point, estimated at 230K for bR (Ferrand et al., 1993). The

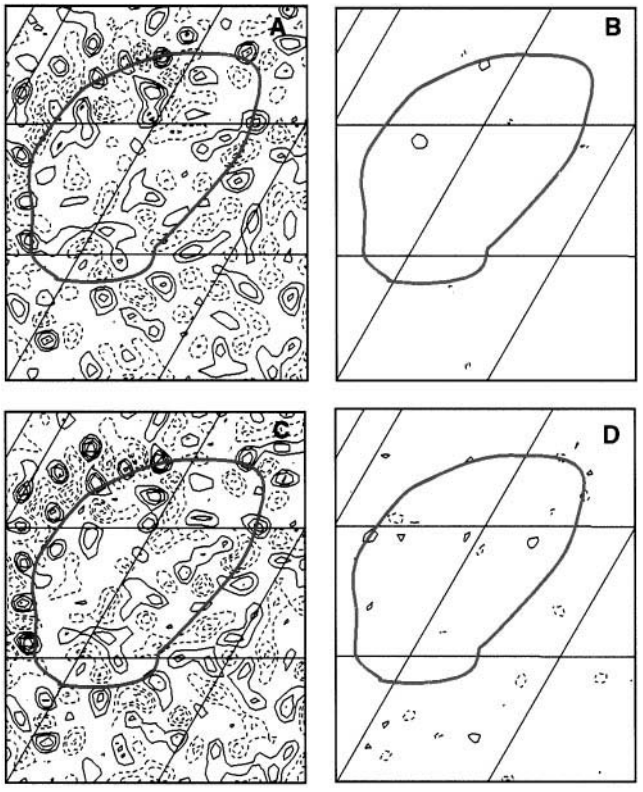

FIGURE 7 Projection map showing light-induced structural changes in bR at 230K and 220K. (*A*) Difference Fourier map obtained from 35 diffraction patterns collected from illuminated samples at 230K (M230K samples), and the same 45 patterns from unilluminated samples at 240K used in Fig. 6. (*B*) Self-difference map obtained from independent halves of the illuminated data set at 230K. (*C*) Difference Fourier map obtained from 48 diffraction patterns collected from illuminated samples at 220K (M220K samples), and the 45 patterns from unilluminated samples at 240K used in Fig. 6. (*D*) Self-difference map obtained from independent halves of the illuminated data set at 220K.

apparent occupancy of peak G1 is especially sensitive to temperature, with appreciable ordering occurring at 220K, even in the absence of photoconversion (Hendrickson and Glaeser, manuscript in preparation). Because the noise levels present in the data are quite low, we consider differences among the three M-minus-bR maps (Figs. 6 *A* and 7, *A* and 7 *C*) to be significant.

DISCUSSION

Sample variation

Some day-to-day variation was detected in the electron microscopy samples we prepared. For example, self-difference maps were less noisy if they were calculated from diffraction data collected from a single grid than if data were pooled from two or more grids, as for the figures shown in this work. A possible source of this variation may lie in the time required for the sample to equilibrate to the target temperature, which can vary between 1 and 10 min. Moreover, we found that diffraction data collected from a few grids, which may have been inadequately humidified, resulted in extremely noisy difference maps with features that were difficult to interpret and were unrelated to previously published work. These data were not used.

Structure of the L intermediate at 170K

Several lines of evidence indicate that the protein structure of bR in the L state must differ from that of bR in the ground state (bR_{568}). The appearance of difference peaks in the amide I and amide II regions in L-minus-BR FTIR difference spectra (e.g., Fig. 3), although modest compared with those present in M-minus-bR spectra, suggests that some movement in the peptide backbone takes place upon formation of the L intermediate. Moreover, studies of site-specific mutants point to a change in the environment of Asp^{115} and Asp^{96} (Braiman et al., 1988, 1991; Gerwert et al. 1989; Maeda et al., 1992), of internal waters (Yamazaki et al., 1995a), and of several aromatic residues (Roepe et al., 1987, 1988) in L. In an incisive set of experiments, Yamazaki et al. (1995b) used the bR mutant W182F along with bR reconstituted with 9-desmethyl retinal to demonstrate that Trp^{182} and the retinal 9-methyl group interact in the L state, possibly in a steric clash. Nevertheless, our electron diffraction projection map shows no difference between the conformation of the L intermediate and that of the ground state (Fig. 2 *B*). Any structural changes present in the L state apparently involve no lateral dispacements large enough to be seen at a resolution of 0.35 nm. Our projection map of the L state does not preclude the possibility that larger protein movements occur in the direction perpendicular to the membrane. In addition, we wish to caution that the L intermediate that is formed at 170K need not be absolutely identical to that formed at physiological temperatures, as Hessling et al. (1993) have already noted.

Identification of photoproducts trapped at 220K, 230K, and 240K from FTIR spectra

The M intermediate of bR is defined as the photoproduct of light-adapted bR that absorbs at ~410 nm, and is therefore yellow, rather than blue or purple like the other intermediates. The use of characteristic absorption spectra in the visible is far more sensitive to the protonation state of the Schiff base than to nuances in protein conformation, however. As a result, the question of how many distinct protein structures evolve between the L state and the N state has been hotly pursued (Varo and Lanyi, 1991a; Ormos et al., 1992; Perkins et al., 1992; Sasaki et al., 1992; Subramaniam et al., 1993; Han et al., 1994; Vonck et al., 1994; Sass et al., 1997; Brown et al., 1997; Nagel et al., 1998). Two key concepts currently influence most thinking on this topic. Varo and Lanyi (1991b) invoked the existence of two M substates, occurring in the sequence $L \leftrightarrow M_1 \rightarrow M_2 \leftrightarrow N$, to explain their observations of photocycle kinetics. In addition, Sasaki et al. (1992) concluded from their studies of

the bR mutant D96N that a third M subtype, the normally transient M_N, immediately precedes N.

Time-resolved FTIR spectra recorded at a point coinciding with maximum absorbance at 410 nm (Souvignier and Gerwert, 1992; Hessling et al., 1993) are in excellent agreement with the "pure M" spectrum published by Ormos et al. (1992), which we, in turn, have used to analyze our FTIR results. In the discussion that follows, we will use the operational term $M_{reference}$ (M_{ref}) to denote this commonly observed M subtype. The relationship between M_{ref} and the kinetically defined subtypes M_1 and M_2 proposed by Varo and Lanyi (1991b) is unknown.

Based on the FTIR spectra presented in this work (Fig. 4), as well as the features of L-, M-, and N-minus-bR_{568} spectra published previously, we identify the photoproducts that we have trapped at 220K, 230K, or 240K, as subtypes of the M intermediate, or admixtures of the same. For convenience we will refer to these photoproducts as M220K, M230K, and M240K.

At 230K and 240K, unambiguous assignments can be made regarding the presence of M_N. Films of bR illuminated at 230K produce FTIR spectra that correlate very highly (0.97) with the spectrum of 95% M_{ref} + 5% N (Ormos et al., 1992) in the key region containing the amide I band (Fig. 5). Hence M230K is equivalent to M_{ref}. Similarly, samples illuminated at 240K show a high correlation with 67% M_{ref} + 33% N in this part of the spectrum. Because the FTIR difference spectrum at 240K can be fully bleached by illumination with blue light (Fig. 4 *A*), and because there is no indication of a protonated Schiff base (such as positive peaks at 1193 cm^{-1} and at 1395 cm^{-1} (Ormos, 1991); compare Fig. 3), the N-like structure present in M240K must be contributed by M_N rather than by N itself.

Structure of the M intermediate in projection at 220K, 230K, and 240K

The FTIR data analyzed in the preceding paragraphs suggest three things: 1) that M220K and M230K are structurally quite similar to each other; 2) that M240 is less like the first two than they are like each other; and 3) that the difference between the structures of M240K and M230K (or M220K) should tell us how the M_{ref} ("true M") and M_N states differ in structure.

Comparison of the Fourier difference projection maps obtained at 240K (Fig. 6 *A*), 230K, and 220K (Fig. 7, *A* and *C*) strongly suggests that helix F begins to tilt even before the N-like signature appears in the FTIR spectrum. This follows from the fact that the F1/F2 positive/negative pair is present in all three maps. This comparison further suggests that helix F is least tilted at 220K and most tilted at 240K. Hence our data suggest that helix F already begins to tilt in the M_{ref} state, an action completed in the subsequent M_N state.

The Fourier difference peak (G1 in Fig. 6 *A*) that has been identified with enhanced ordering of helix G in the M state (Subramaniam et al., 1993) also changes in the three M-minus-bR_{568} difference maps presented here (Figs. 6 *A* and 7, *A* and *C*). The contour height of G1 differs little among the three maps. However, its shape changes more than other peaks nearby, being broadest at 240K and seemingly pinched into two separate peaks at 220K. Lacking three-dimensional data for these samples, we can offer no interpretation at this time.

There are additional structural changes in the protein that occur in the M_{ref} state, remote from helices F and G. Portions of helices B and either D or E, or both, apparently undergo a structural readjustment when the M intermediate is formed. A positive/negative pair (our peaks B1 and DE2) in this region is present in most M- and N-minus-bR_{568} difference maps published thus far (Dencher et al., 1989; Nakasako et al., 1991; Subramaniam et al., 1993; Han et al., 1994; Vonck, 1996; Kamikubo et al., 1996; Sass et al., 1997), but no structural interpretation has been offered. We suggest that helices at the interface between monomers may repack themselves in the M state. However, further understanding must await the more complete, three-dimensional information that can be obtained from tilted specimens.

Several well-defined peaks appear outside the protein envelope at identical positions in all three of our M-minus-bR_{568} difference maps (Figs. 6 *A* and 7, *A* and *C*), whereas none are present in our L-minus-bR_{568} map (Fig. 2 *B*). The negative peak labeled L2 in Fig. 6 *A* coincides with the projection of lipid 269 in the atomic model of purple membrane published by Grigorieff et al. (1996); peak L1 presumably represents the movement of this lipid to a new position, possibly in response to the structural change in nearby helix G.

We believe that the peaks in the lipid region represent an authentic response to light-induced changes in protein structure. Of course, one may argue that it is the dehydration of the specimen by the heat of illumination that causes the systematic structural changes that we detect in the lipid region. However, in bR_{568}-minus-bR_{568} difference maps for samples equilibrated at different temperatures, there is less pronounced but clear evidence of repositioning and ordering of lipids (Hendrickson and Glaeser, manuscript in preparation). Photoconversion to the M state enhances the lipid peaks, and does so most strongly at 220K, where thermal effects from illumination should be least effective.

Do M220K, M230K, and M240K recapitulate a temporal sequence in the photocycle that takes place under physiological conditions? Such an interpretation is justified for M230K and M240K, because the FTIR signature of M240K is consistent with a mixed population in which some molecules have the "true M" (M_{ref}) structure of M230K, whereas others have the N-like structure of M_N (Fig. 5). Alternatively, M240K may represent a distinct, transitional step between M230K and M_N. In any case, the implication is that the transition from M_{ref} to M_N primarily involves helices F and G.

Getting from L to N

By varying the hydration of their purple membrane samples, Sass et al. (1997) and Kamikubo et al. (1997) have also sought to characterize the structural changes undergone by bR in the M state. Because their samples were prepared without glucose and at pH 10, comparison of our results with theirs is not straightforward. Nevertheless, it is apparent that the FTIR difference spectra that they obtain for the bR mutant D96N at 75% and 100% r.h., respectively, is similar to our difference spectrum for wild type at 240K, 81% r.h. (Fig. 4 *A*, *top*). It is reassuring, therefore, that the Fourier difference map that both groups calculate for that sample has an F2 peak with the extended shape seen only at 240K in our difference maps (Fig. 6 *A*).

It is intriguing that Sass and co-workers trap an M subtype at r.h. $\leq$ 57% with few if any large-scale structural changes. Another example of an M intermediate lacking the familiar conformational changes in helices F and G is the species trapped using the bR mutant D38R (personal communication from M. Lindahl, Max Planck Institute, Frankfurt). This M species may represent the protein structure formed at a point immediately after the deprotonation of the Schiff base; by analogy to M_N, it might be called M_L. Assuming that large-scale conformational changes first occur in the $M_L \rightarrow$ M220K transition, it would appear that such changes must result from the disruption of the interaction of the Schiff base with the complex counterion rather than from retinal isomerization, in agreement with the proposal of Brown et al. (1997).

The earliest structural changes that we detect, at 220K, include some movement of helix F as well as a change in helix G. In the transition from M220K to M_{ref} (which forms at 230K) and from M_{ref} to M_N, helix F undergoes further structural adjustments, which may include an increase in tilt angle.

How, then, does bR spontaneously return to the resting state? Beyond the N intermediate, the progression of the photocycle is poorly understood at a structural level. Further diffraction studies that probe the structure of the O intermediate, like those presented by Subramaniam et al. (1997), will be needed to complete the picture.

We thank Janet Vonck for developing some of the protocols used in this work, Eric Wunderlich for helping with data processing, and Ken Downing for a great deal of practical advice, as well as a critical reading of a preliminary draft of the manuscript. We are indebted to Richard Henderson and Janos Lanyi for many insightful discussions and for sharing results in advance of publication. Strain ET1001 of *H. salinarium* was a gift from Richard Mathies.

REFERENCES

Ames, J. B., S. P. A. Fodor, R. Gebhard, J. Raap, E. M. M. van den Berg, J. Lugtenburg, and R. A. Mathies. 1989. Bacteriorhodopsin's M412 intermediate contains a 13-*cis*,14-s-*trans*,15-*anti*-retinal Schiff base chromophore. *Biochemistry*. 28:3681–3687.

Baldwin, J., and R. Henderson. 1984. Measurement and evaluation of electron diffraction patterns from two-dimensional crystals. *Ultramicroscopy.* 14:319–336.

Braiman, M. S., O. Bousche, and K. J. Rothschild. 1991. Protein dynamics in the bacteriorhodopsin photocycle: submillisecond Fourier transform infrared spectra of the L, M, and N photointermediates. *Proc. Natl. Acad. Sci. USA.* 88:2388–2392.

Braiman, M., and R. Mathies. 1980. Resonance Raman evidence for an all-*trans* to 13-*cis* isomerization in the proton-pumping cycle of bacteriorhodopsin. *Biochemistry.* 19:5421–5428.

Braiman, M. S., T. Mogi, T. Marti, L. J. Stern, H. G. Khorana, and K. J. Rothschild. 1988. Vibrational spectroscopy of bacteriorhodopsin mutants: light-driven proton transport involves protonation changes of aspartic acid residues 85, 96, and 212. *Biochemistry.* 27:8516–8520.

Brown, L. S., Y. Gat, M. Sheves, Y. Yamazaki, A. Maeda, R. Needleman, and J. K. Lanyi. 1994. The retinal Schiff base-counterion complex of bacteriorhodopsin: changed geometry during the photocycle is a cause of proton transfer to aspartate 85. *Biochemistry.* 33:12001–12011.

Brown, L. S., H. Kamikubo, L. Zimanyi, M. Kataoka, F. Tokunaga, P. Verdegem, J. Lugtenburg, and J. K. Lanyi. 1997. A local electrostatic change is the cause of the large-scale protein conformation shift in bacteriorhodopsin. *Proc. Natl. Acad. Sci. USA.* 94:5040–5044.

Brown, L. S., J. Sasaki, H. Kandori, A. Maeda, R. Needleman, and J. K. Lanyi. 1995. Glutamic acid 204 is the terminal proton release group at the extracellular surface of bacteriorhodopsin. *J. Biol. Chem.* 270: 27122–27126.

Ceska, T. A., and R. Henderson. 1990. Analysis of high-resolution electron diffraction patterns from purple membrane labelled with heavy-atoms. *J. Mol. Biol.* 213:539–560.

Dencher, N. A., D. Dresselhaus, G. Zaccai, and G. Buldt. 1989. Structural changes in bacteriorhodopsin during proton translocation revealed by neutron diffraction. *Proc. Natl. Acad. Sci. USA.* 86:7876–7879.

Ebrey, T. G. 1993. Light energy transduction in bacteriorhodopsin. *In* Thermodynamics of Membrane Receptors and Channels. M. B. Jackson, editor. CRC Press, Boca Raton, FL. 354–387.

Farrar, M. R., K. V. Lakshmi, S. O. Smith, R. Brown, J. Raap, J. Lugtenburg, R. G. Griffin, and J. Herzfeld. 1993. Solid-state NMR study of [ϵ-^{13}C] lys-bacteriorhodopsin: Schiff base photoisomerization. *Biophys. J.* 65:310–315.

Ferrand, M., A. J. Dianoux, W. Petry, and G. Zaccai. 1993. Thermal motions and function of bacteriorhodopsin in purple membranes: effects of temperature and hydration studied by neutron scattering. *Proc. Natl. Acad. Sci. USA.* 90:9668–9672.

Fodor, S. P. A., J. B. Ames, R. Gebhard, E. M. M. van den Berg, W. Stoeckenius, J. Lugtenburg, and R. A. Mathies. 1988a. Chromophore structure in bacteriorhodopsin's N intermediate: implications for the proton-pumping mechanism. *Biochemistry.* 27:7097–7101.

Fodor, S. P. A., W. T. Pollard, R. Gebhard, E. M. M. van den Berg, J. Lugtenburg, and R. A. Mathies. 1988b. Bacteriorhodopsin's L550 intermediate contains a C14–C15 s-*trans*-retinal chromophore. *Proc. Natl. Acad. Sci. USA.* 85:2156–2160.

Gerwert, K., B. Hess, J. Soppa, and D. Oesterhelt. 1989. Role of aspartate-96 in proton translocation by bacteriorhodopsin. *Proc. Natl. Acad. Sci. USA.* 86:4943–4947.

Grigorieff, N., T. A. Ceska, K. H. Downing, J. M. Baldwin, and R. Henderson. 1996. Electron-crystallographic refinement of the structure of bacteriorhodopsin. *J. Mol. Biol.* 259:393–421.

Han, B.-G., J. Vonck, and R. M. Glaeser. 1994. The bacteriorhodopsin photocycle: direct structural study of two substates of the M-intermediate. *Biophys. J.* 67:1179–1186.

Henderson, R., J. M. Baldwin, T. A. Ceska, F. Zemlin, E. Beckmann, and K. H. Downing. 1990. Model for the structure of bacteriorhodopsin based on high-resolution electron cyro-microscopy. *J. Mol. Biol.* 213: 899–929.

Hessling, B., G. Souvignier, and K. Gerwert. 1993. A model-independent approach to assigning bacteriorhodopsin's intramolecular reactions to photocycle intermediates. *Biophys. J.* 65:1929–1941.

Kamikubo, H., M. Kataoka, G. Varo, T. Oka, F. Tokunaga, R. Needleman, and J. Lanyi. 1996. Structure of the N intermediate of bacteriorhodopsin revealed by x-ray diffraction. *Proc. Natl. Acad. Sci. USA.* 93: 1386–1390.

Kamikubo, H., T. Oka, Y. Imamoto, F. Tokunaga, J. K. Lanyi, and M. Kataoka. 1997. The last phase of the preprotonation switch in bacteriorhodopsin: the transition between the M-type and the N-type protein conformation depends on hydration. *Biochemistry*. 36: 12282–12287.

Kimura, Y., D. G. Vassylyev, A. Miyazawa, A. Kidera, M. Matsushima, K. Mitsuoka, K. Murata, T. Hirai, and Y. Fujiyoshi. 1997. Surface of bacteriorhodopsin revealed by high-resolution electron crystallography. *Nature*. 389:206–211.

Koch, M. H. J., N. A. Dencher, D. Oesterhelt, H.-J. Plohn, G. Rapp, and G. Buldt. 1991. Time-resolved x-ray diffraction study of structrual changes associated with the photocycle of bacteriorhodopsin. *EMBO J.* 10: 521–526.

Lanyi, J. K. 1993. Proton translocation mechanism and energetics in the light-driven pump bacteriorhodopsin. *Biochim. Biophys. Acta.* 1183: 241–261.

Litvin, F. F., and S. P. Balashov. 1977. New intermediates in the photochemical transformation of bacteriorhodopsin. *Biofizika.* 22:1111–1114.

Lozier, R. H., R. A. Bogomolni, and W. Stoekenius. 1975. Bacteriorhodopsin: a light-driven proton pump in *Halobacterium halobium. Biophys. J.* 15:955–962.

Maeda, A., J. Sasaki, Y. Shichida, T. Yoshizawa, M. Chang, B. Ni, R. Needleman, and J. K. Lanyi. 1992. Structures of aspartic acid-96 in the L and N intermediates of bacteriorhodopsin: analysis by Fourier transform infrared spectroscopy. *Biochemistry.* 31:4684–4690.

Mathies, R. A., S. W. Lin, J. B. Ames, and W. T. Pollard. 1991. From femtoseconds to biology: mechanism of bacteriorhodopsin's light-driven proton pump. *Annu. Rev. Biophys. Biophys. Chem.* 20:491–518.

Mohr, S. C., W. D. Wilk, and G. M. Barrow. 1965. The association of water with bases and anions in an inert solvent. *J. Am. Chem. Soc.* 87:3048–3052.

Nagel, G., B. Kelety, B. Mockel, G. Buldt, and E. Bamberg. 1998. Voltage dependence of proton pumping by bacteriorhodopsin is regulated by the voltage-sensitive ratio of M1 to M2. *Biophys. J.* 74:403–412.

Nakasako, N., M. Kataoka, Y. Amemiya, and F. Tokunaga. 1991. Crystallographic characterization by x-ray diffraction of the M-intermediate from the photo-cycle of bacteriorhodopsin at room temperature. *Fed. Eur. Biochem. Soc. Lett.* 292:73–75.

Oesterhelt, D., and W. Stoeckenius. 1974. Isolation of the cell membrane of *Halobacterium halobium* and its fractionation into red and purple membrane. *Methods Enzymol.* 31:667–678.

Ormos, P. 1991. Infrared spectroscopic demonstration of a conformational change in bacteriorhodopsin involved in proton pumping. *Proc. Natl. Acad. Sci. USA.* 88:473–477.

Ormos, P., K. Chu, and J. Mourant. 1992. Infrared study of the L, M, and N intermediates of bacteriorhodopsin using the photoreaction of M. *Biochemistry.* 31:6933–6937.

Pebay-Peyroula, E., G. Rummel, J. Rosenbusch, and E. M. Landau. 1997. X-ray structrue of bacteriorhodopsin at 2.5 angstroms from microcrystals grown in lipidic cubic phases. *Science.* 277:1676–1681.

Perkins, G. A., E. Liu, F. Burkard, E. A. Gerry, and R. M. Glaeser. 1992. Characterization of the conformational change in the M1 and M2 substates of bacteriorhodopsin by the combined use of visible and infrared spectroscopy. *J. Struct. Biol.* 109:142–151.

Roepe, P., P. L. Ahl, S. K. Das Gupta, J. Herzfeld, and K. J. Rothschild. 1987. Tyrosine and carboxyl protonation changes in the bacteriorhodopsin photocycle 1. M_{412} and L_{550} intermediates. *Biochemistry.* 26: 6696–6707.

Roepe, P., D. Gray, J. Lugtenburg, E. M. M. van den Berg, J. Herzfeld, and K. J. Rothschild. 1988. FTIR evidence for tryptophan perturbations during the bacteriorhodopsin photocycle. *J. Am. Chem. Soc.* 110: 7223–7224.

Rothschild, K. J. 1992. FTIR difference spectroscopy of bacteriorhodopsin: toward a molecular model. *J. Bioenerg. Biomembr.* 24:147–167.

Rothschild, K. J., and S. Sonar. 1995. Bacteriorhodopsin: new biophysical perspectives. *In* CRC Handbook of Organic Photochemistry and Photobiology. W. M. Horspool, editor. CRC Press, Boca Raton, FL. 1521–1544.

Sasaki, J., Y. Shichida, J. K. Lanyi, and A. Maeda. 1992. Protein changes associated with reprotonation of the Schiff base in the photocycle of $Asp^{96} \rightarrow$ Asn bacteriorhodopsin. *J. Biol. Chem.* 267:20782–20786.

Sass, H. J., I. W. Schachowa, G. Rapp, M. H. J. Koch, D. Oesterhelt, G. Buldt, and N. A. Dencher. 1997. The tertiary structural changes in bacteriorhodopsin occur between M states: x-ray diffraction and Fourier transform infrared spectroscopy. *EMBO J.* 16:1484–1491.

Smith, S. O., J. A. Pardoen, P. P. J. Mulder, B. Curry, J. Lugtenburg, and R. Mathies. 1983. Chromophore structure in bacteriorhodopsin's O_{640} photointermediate. *Biochemistry.* 22:6141–6148.

Souvignier, G., and K. Gerwert. 1992. Proton uptake mechanism of bacteriorhodopsin as determined by time-resolved stroboscopic-FTIR-spectroscopy. *Biophys. J.* 63:1393–1405.

Subramaniam, S., A. R. Faruqi, D. Oesterhelt, and R. Henderson. 1997. Electron diffraction studies of light-induced conformational changes in the $Leu^{93} \rightarrow$ Ala bacteriorhodopsin mutant. *Proc. Natl. Acad. Sci. USA*. 94:1767–1772.

Subramaniam, S., M. Gerstein, D. Oesterhelt, and R. Henderson. 1993. Electron diffraction analysis of structural changes in the photocycle of bacteriorhodopsin. *EMBO J.* 12:1–8.

Varo, G., and J. K. Lanyi. 1991a. Kinetic and spectroscopic evidence for an irreversible step between deprotonation and reprotonation of the Schiff base in the bR photocycle. *Biochemistry.* 30:5008–5015.

Varo, G., and J. K. Lanyi. 1991b. Thermodynamics and energy coupling in the bR photocycle. *Biochemistry.* 30:5016–1022.

Vonck, J. 1996. A three-dimensional difference map of the N intermediate in the bacteriorhodopsin photocycle: part of the F helix tilts in the M to N transition. *Biochemistry.* 35:5870–5878.

Vonck, J., B.-G. Han, F. Burkard, G. A. Perkins, and R. M. Glaeser. 1994. Two progressive substates of the M-intermediate can be identified in glucose-embedded, wild-type bacteriorhodopsin. *Biophys. J.* 67: 1173–1178.

Yamazaki, Y., M. Hatanaka, H. Kandori, J. Sasaki, W. F. J. Karstens, J. Raap, J. Lugtenburg, M. Bizounok, J. Herzfeld, R. Needleman, J. K. Lanyi, and A. Maeda. 1995a. Water structural changes at the proton uptake site (the Thr^{46}-Asp^{96} domain) in the L intermediate of bacteriorhodopsin. *Biochemistry.* 34:7088–7093.

Yamazaki, Y., J. Sasaki, M. Hatanaka, H. Kandori, A. Maeda, R. Needleman, T. Shinada, K. Yoshihara, L. S. Brown, and J. K. Lanyi. 1995b. Interaction of tryptophan-182 with the retinal 9-methyl group in the L intermediate of bacteriorhodopsin. *Biochemistry.* 34:577–582.